www.czasopisma.pan.pl PAN www.journals.pan.pl
Chemical and Process Engineering 2020, 41 (1), 45–57
DOI: 10.24425/cpe.2019.130222

VERIFICATION OF MODELS OF GAS BUBBLE BREAK-UP CAUSED BY EDDIES GENERATED BY A SELF-ASPIRATING DISK IMPELLER

Jacek Stelmach*, Radosław Musowski

Lodz University of Technology, Faculty of Process and Environmental Engineering,
Wolczanska 213, 90-924 Lodz, Poland

The paper presents a photographic analysis of the break-up of gas bubbles flowing out of the outlets of a self-aspirating disk impeller. It was found that bubbles detached from the interfacial surface most often disintegrate to form several daughter bubbles. Further in the work, the population balance model was verified for several formulas describing the bubble break-up rate. It has been found that a good fit to the experimental data is provided by the formula given by Laakkonen for 5 daughter bubbles. The possibility of using the Monte Carlo method to model the bubble break-up process was also determined. For this method, a good agreement of results was achieved for the division into a maximum of 10 daughter bubbles. In the case of this method it was also found necessary to use the function of break-up frequency at a higher rate for smaller bubbles.

Keywords: self-aspirating disk impeller, bubble break-up, population balance model

1. INTRODUCTION

Mechanical mixing with simultaneous gas dispersion is a process often used in industry. Self-aspirating (gas inducing) impellers allow this process to be carried out without the use of gas-compressing devices, which simplifies the construction of the installation. Their disadvantage is the dependence of gas stream on the rotational frequency and height of liquid above the impeller. It was also found that bubble sizes increased with the increase of rotational frequency of the self-aspirating impeller. This phenomenon is unfavourable from the point of view of the mass transfer process and requires a more thorough examination. A certain facilitation in the cognitive process may be mathematical modelling of the processes of break-up and coalescence of gas bubbles in a liquid.

Recently, many solutions based on the population balance model were presented with the classification of bubbles into size classes. Further simplification of the model can be obtained by assuming the lack of coalescence. This situation occurs in the initial phase of self-aspiration, when the number of bubbles is low and the likelihood of bubble collisions is very small. Then, for size classes, the model equation has the form (Alopaeus et al., 1999):

$$\frac{dY_i}{dt} = Y_{i,in} + \sum_{j=i+1}^{n_c} \nu\left(d_i\right) \cdot \beta\left(d_i, d_j\right) \cdot g\left(d_j\right) \cdot Y_j \cdot \Delta d - Y_{i,out} - g\left(d_i\right) \cdot Y_i \tag{1}$$

The bubble break-up frequency $g(d)$ can be calculated from several equations described in the literature on the subject. Martinez-Bazán et al. (1999) and Kálal et al. (2014) proposed the following bubble break-up

* Corresponding author, e-mail: jacek.stelmach@p.lodz.pl

model:

$$g\left(d_i\right) = K_g \cdot \frac{\sqrt{\beta \cdot \left(\varepsilon \cdot d_i\right)^{2/3} - \dfrac{12 \cdot \sigma}{\rho_C \cdot d_i}}}{d_i} \tag{2}$$

Constants K_g and β are equal to 0.25 and 8.2, respectively.

Lehr et al. (2002) proposed another equation describing the frequency of gas bubble break-up:

$$\left(d_i\right) = \frac{1}{2} \cdot \frac{d_i^{5/3} \cdot \varepsilon^{19/15} \cdot \rho_C^{7/5}}{\sigma^{7/5}} \exp\left(-\frac{\sqrt{2} \cdot \sigma^{9/5}}{d_i^3 \cdot \rho_C^{9/5} \cdot \varepsilon^{6/5}}\right) \tag{3}$$

In turn, Laakkonen et al. (2007) presented the equation:

$$g\left(d_i\right) = C_1 \cdot \varepsilon^{1/3} \cdot \operatorname{erfc}\left(\sqrt{\mathrm{C}_2 \frac{\sigma}{\rho_\mathrm{C} \cdot \varepsilon^{2/3} \cdot \mathrm{d}_\mathrm{i}^{5/3}} + \mathrm{C}_3 \frac{\eta_\mathrm{C}}{\sqrt{\rho_\mathrm{C} \cdot \rho_\mathrm{D}} \cdot \varepsilon^{1/3} \cdot \mathrm{d}_\mathrm{i}^{4/3}}}\right) \tag{4}$$

combining bursting forces with those that prevent bubble break-up. This equation gives good results in stirred tanks (Kálal et al., 2014), and the experimentally determined constant values are $C_1 = 2.52$, $C_2 = 0.04$, $C_3 = 0.01$ (Laakkonen et al., 2006).

Figure 1 presents bubble break-up frequencies calculated from Eqs. (2), (3) and (4) depending on bubble diameter for energy dissipation rate $\varepsilon = 16$ m^2/s^3 (this value is very likely near the blades of this impeller (Stelmach et al., 2019)). The analysis of Fig. 1 shows that bubble break-up frequencies calculated from these equations differ by almost two orders of magnitude (approximately one hundred times) for bubbles larger than 2 mm. For very small bubbles Eq. (3) gives lower break-up frequencies. In addition, Eq. (2) becomes indefinite for bubble size smaller than the critical one $d_c = 1.26 \cdot (\sigma/\rho_C)^{3/5} \cdot \varepsilon^{-2/5}$. In the discussed case this occurs for bubbles smaller than 1.36 mm, but at lower values of ε indefiniteness will occur for larger bubble sizes (e.g. for $\varepsilon = 2$ m^2/s^3, $d_c = 3.12$ mm). However, in the tank there may be bubbles which are smaller than the critical ones, as they may form as a result of division.

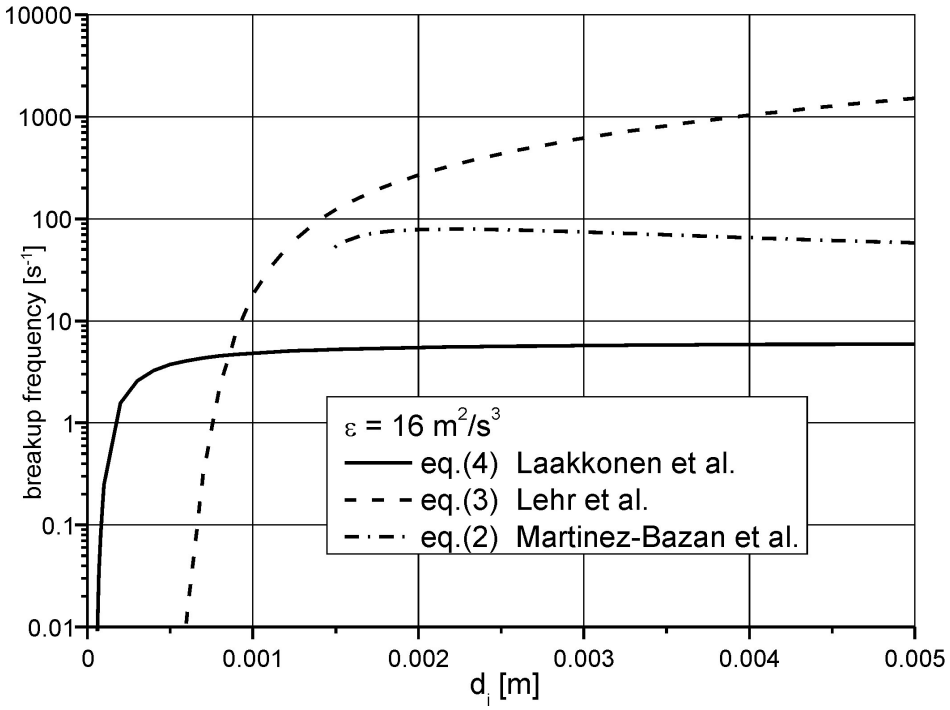

Fig. 1. Bubble break-up frequency

Important data for calculations are the number of daughter bubbles $n(d_i)$ and daughter size distribution (DSD) $\beta(d_i, d_j)$. The simplest case of calculations is the division into two bubbles of equal volume. However, it is energetically unfavorable and binary division into bubbles of unequal volumes is often assumed (Attarakih et al., 2009). According to literature (Laakkonen et al., 2007), the binary division occurs in 48% of cases. In 37% of observations, however, there is a division into 3 to 7 fragments (daughter bubbles).

Many equations have been proposed for the calculation of DSD (Alopaeus et al., 1999; Hengel et al., 2005; Kálal et al., 2014; Luo and Svendsen, 1996). One of the oldest is

$$\beta\left(d_i, d_j\right) = 90 \cdot \frac{d_i^2}{d_j^3} \cdot \left(\frac{d_i^3}{d_j^3}\right)^2 \cdot \left(1 - \frac{d_i^3}{d_j^3}\right)^2 \tag{5}$$

then developed into the form

$$\beta\left(d_i, d_j\right) = \frac{1}{2} \cdot (1 + C_4) \cdot (2 + C_4) \cdot (3 + C_4) \cdot (4 + C_4) \cdot \left(\frac{d_i^2}{d_j^3}\right) \cdot \left(\frac{d_i^3}{d_j^3}\right)^2 \cdot \left(1 - \frac{d_i^3}{d_j^3}\right)^{C_4} \tag{6}$$

for binary division $C_4 = 2$, while for the division into many daughter bubbles $C_4 = 18.25$. Figure 2 shows the probability of forming a bubble of diameter d_i if bubbles of diameters $d_j = 1$ mm, 3 mm and 5 mm are divided.

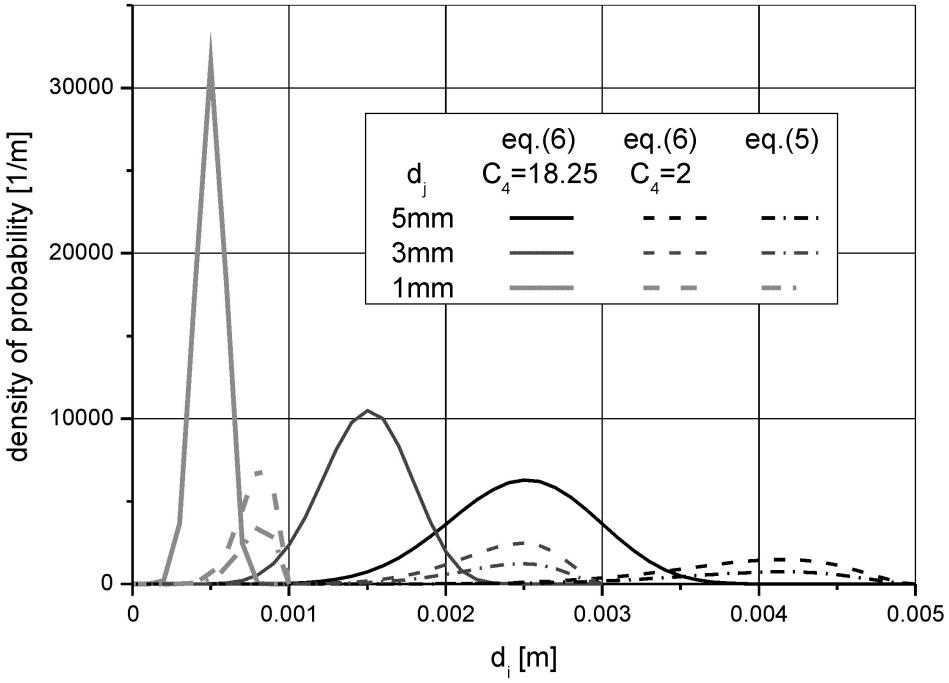

Fig. 2. Probability of the formation of a bubble of diameter d_j during division of a bubble of diameter d_j

Because Eq. (1) is iteratively solved in a numerical way, another method for determining the size of daughter bubbles is random determination, while maintaining the condition of equal volumes of the primary and daughter bubbles. This is a method known as the Monte Carlo method (MC).

Model calculations are verified by comparing the results of calculations with experimental data. For the self-aspirating disk impeller the probability density distribution of bubble sizes in the initial stage of self-aspiration was determined (Stelmach, 2006; 2007). The results obtained are presented in Fig. 3 which also shows the values of Sauter diameters d_{32}.

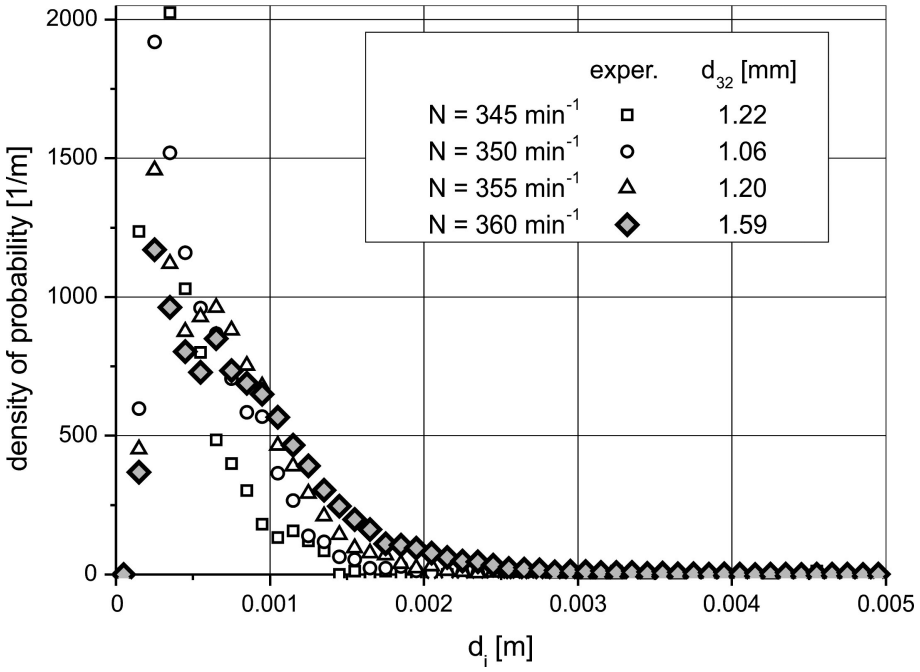

Fig. 3. Probability density distribution of bubble sizes at the beginning of self-aspiration

The aim of the work is to verify the applicability of the population balance model (1) using different bubble break-up rates for a self-aspirating disk impeller assuming that

- bubbles of the same size, i.e. d_{in} = const., are detached from the interfacial surface,
- there is no outflow of bubbles during their break-up, i.e. $Y_{i,out} = 0\ s^{-1}$,
- the energy dissipation rate is constant (ε = const.) in the entire bubble break-up area.

2. MEASUREMENTS

The measurements were made in a flat-bottomed glass tank of diameter $T = 0.292$ m equipped with four baffles of width $B = 0.1{\cdot}T$. A self-aspirating disk impeller of diameter $D = 0.125$ m was placed at height $h = 0.075$ m over the bottom of the tank. The tank was filled with water ($t = 20$ °C) to height $H = 0.3$ m. To reduce optical distortions, a cylindrical tank was placed in a rectangular tank, and the space between tank walls was filled with water. Rotational frequency of the impeller was $N = 6\ s^{-1}$. Under the measurement conditions, the Reynolds number was $Re = 93580$, and the modified Froude number was $Fr' = 0.255$. This is the initial phase of self-aspirating (self-inducing) because for the tested impeller the gas dispersion begins at $Fr' = 0.210$. On the basis of previous studies, in these conditions the gas hold-up was $\Phi = 0.47\%$, and the stream of dispersed gas was $V_G = 2.34 \cdot 10^{-5}\ m^3/s$ (Stelmach, 2000). The mean residence time of air bubbles in the liquid calculated on this basis was $\tau = 4.06$ s.

2.1. Outflow of bubbles

In the observations of phenomena taking place during the outflow of bubbles from the outlets, a RedLake camera with resolution of 480 px × 420 px was used. The camera was placed under the bottom of the tank and with the help of a computer it recorded images with frequency 250 fr/s. Two 1000 W halogen lamps were used to illuminate the tank inside. The interior of the tank was illuminated from the sides by light tunnels 0.015 m high. In these measurements, an agitator made of plexiglass was used to observe the detachment of bubbles from the interfacial surface inside the outlet.

2.2. Energy dissipation rate

Energy dissipation rate was determined based on the measurements of instantaneous liquid velocities in the tank using the PIV method. At a very small amount of gas in the liquid bubbles virtually have no effect on the motion of gas phase. Therefore, in these measurements the impeller worked without gas dispersion. The absence of gas phase makes liquid velocity measurements much easier.

The measurements by the PIV method were made using a LaVision system with the Nd:YAG laser of maximum power 135 mW. A light knife about 1 mm thick was in the plane determined by the tank axis and bisector of the angle between the baffles. An ImagePro camera with resolution 2048 px × 2048 px equipped with Nikkor 1.8/50 lens was placed perpendicular to the light knife. The measuring field was 60 mm × 60 mm. Laser pulses were initiated by an external trigger when the blade was 5°, 10° and 15° behind the plane of the light knife. The scheme of the experimental rig is analogous to that in our other paper devoted to the distribution of turbulent energy dissipation rate near the tested impeller (Stelmach et al., 2019).

A series of 200 images were taken and then processed using the DaVis 7.2 software. Two-pass data processing with interrogation area of 32 px × 32 px without overlaying was used. Instantaneous velocity distributions in the measurement area and velocity distributions of average and mean square velocity pulsations (in the RMS sense) were obtained. These data were used to calculate energy dissipation rates from dimensional equation and the Smagorinsky model.

3. RESULTS AND DISCUSSION

3.1. Outflow of bubbles

Figure 4 shows a sequence of images illustrating the way bubbles are detached from the interfacial surface inside the impeller and disintegrate into smaller fragments. Analysis of subsequent frames shows that the bubbles first detach from the interfacial surface inside the impeller. Diameters of these bubbles reach up to 5 mm. This value is consistent with the size of the ventilated cavern calculated on the basis of the formula given by Paglianti et al. (2006). Then, these bubbles are disintegrated by eddies behind the impeller blade, and more than two daughter bubbles may be formed. Bubble shapes during their break-up deviate from spherical ones. On the other hand, small bubbles that have been formed in the break-up process do have spherical shapes (Stelmach, 2006). It can also be seen that the breaking of bubbles occurs only under the influence of eddies in the space behind impeller blades (Stelmach et al., 2016). The blades themselves do not cause mechanical breaking of the bubbles at the tested rotational frequency of the impeller. Therefore, similarity to processes taking place in air-lift column reactors can be found (Pohorecki et al., 2001a; 2001b). Previous studies (Stelmach and Kuncewicz, 2011) have also found that there are significant differences in liquid velocities (the first of all tangential components) and gas bubbles in the area of bubble disintegration.

It follows from the observations that the breaking process lasts no longer than about 1/6 of the impeller rotation, which for rotational frequency $N = 6\ \mathrm{s}^{-1}$ is $\tau = 0.028$ s. This value is therefore a time limit for the modelling process – at this time the bubble size distribution should be as close to the experimental one as possible.

Two diameters of bubbles leaving the opening were assumed for the model calculation, i.e. $d_{in} = 3$ mm (most probable) and $d_{in} = 5$ mm (maximum). This gives the number of 1655 and 376 bubbles flowing out of the impeller outlet orifices per second, respectively. These values were calculated on the basis of the dependence of volume gas flow from the rotational frequency of the impeller (Stelmach, 2000).

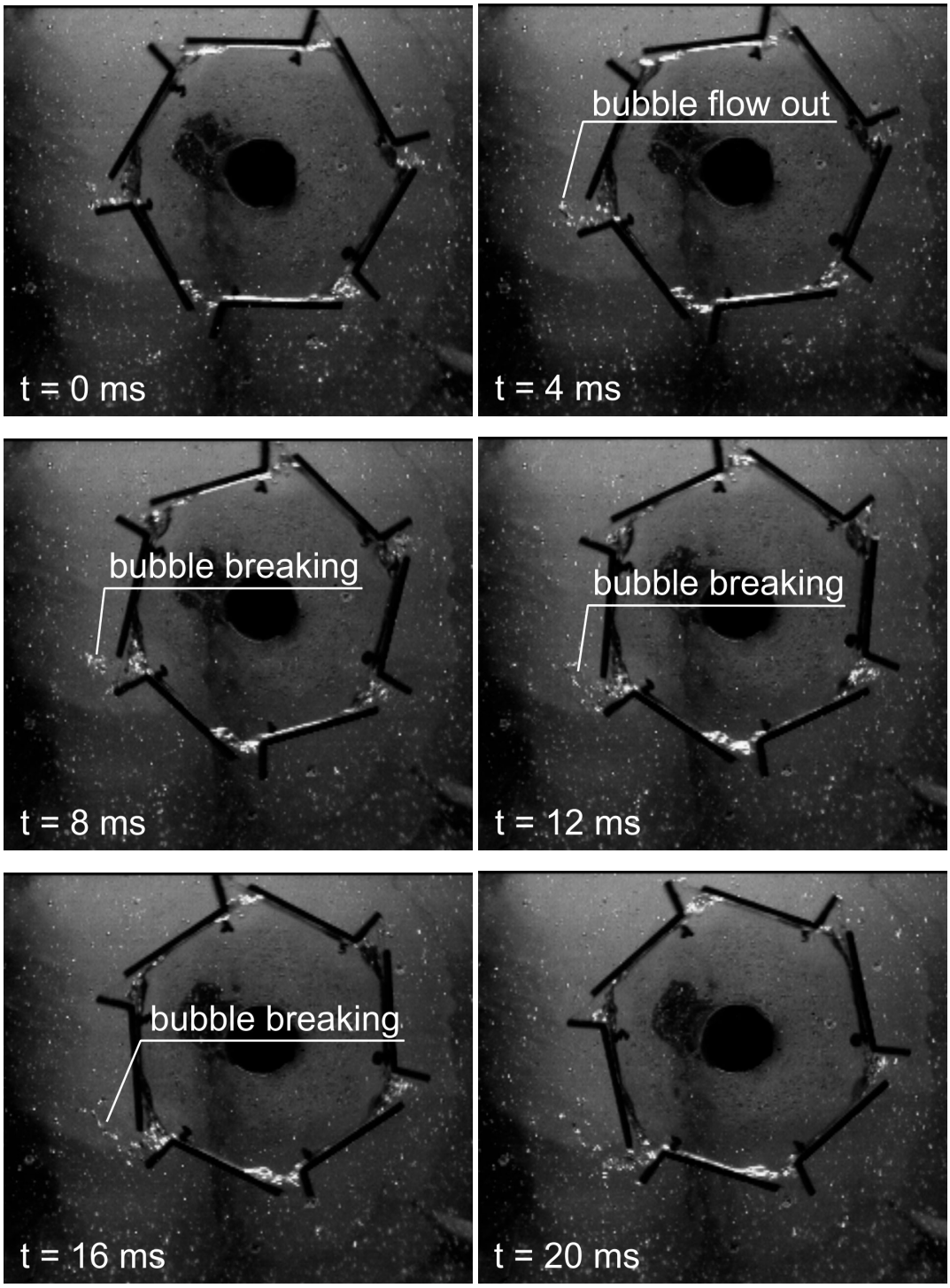

Fig. 4. Outflow and break-up of bubbles

3.2. Distribution of energy dissipation rate

As has been shown previously, the breaking of bubbles takes place in the space behind the impeller blade. To calculate the bubble break-up rate, it is necessary to know energy dissipation rate ε in the space in which the breaking process takes place. To determine this rate distribution, the following equations were used:

$$\varepsilon = C\frac{\overline{u}'^3}{D} \tag{7}$$

and

$$\varepsilon = (C_s \cdot \Delta l)^2 \cdot \overline{\left[\frac{1}{2} \cdot \left(\frac{\partial u_i'}{\partial x_j} + \frac{\partial u_j'}{\partial x_i}\right)^2\right]^{3/2}} \tag{8}$$

assuming isotropic turbulence. Coefficient C in Eq. (7) equals 5.2 (Kania and Kuncewicz, 2002). In a recent study (Stelmach et al., 2019) the value of Smagorinski constant for the tested impeller was determined at $C_s = 0.07$. The assumption of isotropic turbulence makes it possible to supplement missing members of Eq. (8). Figures 5 and 6 show the distributions of energy dissipation rate near the impeller, 10° and 15° behind its blade, calculated from both equations (detailed distributions of ε near the impeller blades are presented in our earlier work (Stelmach et al., 2019)). In the figures, areas with the most intense bubble break-ups are marked with a frame. For these areas, mean values were calculated. However, from analysis of Fig. 4 it follows that most of the break-ups take place in the area where the energy dissipation rate is the highest. In the presence of gas phase under the measuring conditions, the values of ε are reduced by no more than 10% (Stelmach, 2014).

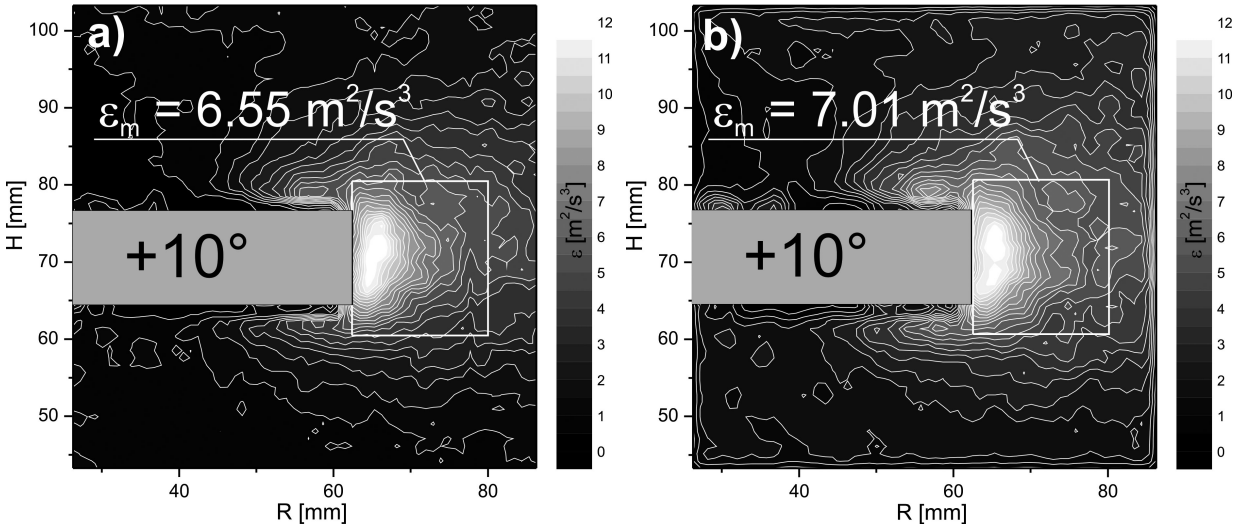

Fig. 5. Distribution of energy dissipation rates 10° behind the blade: a) from Eq. (7), b) from Eq. (8)

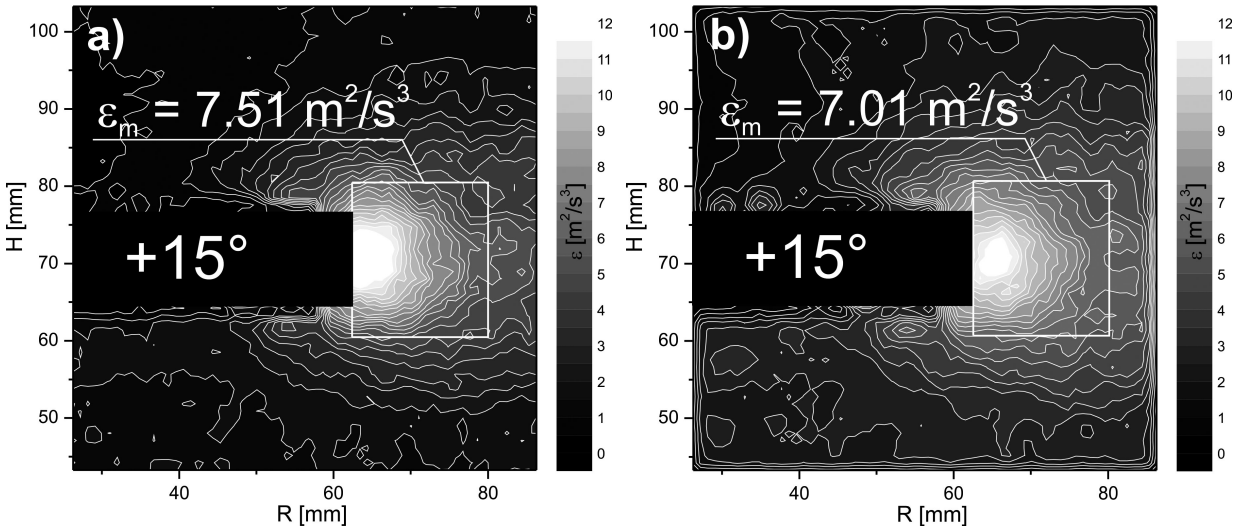

Fig. 6. Distribution of energy dissipation rates 15° behind the blade: a) from Eq. (7), b) from Eq. (8)

3.3. Bubble size distributions for binary break-up

Determination of the energy dissipation rate in the vicinity of the impeller allowed us to calculate the bubble size distribution during break-up into two daughter bubbles. Figure 7 presents probability density distributions of bubble size calculated from Eqs. (3) and (4) for the initial diameter of 3 mm and four energy dissipation rates (2, 4, 8 and 16 m^2/s^3). From Eq. (6) the diameter of a bubble whose formation is most probable has been determined. The diameter of the other bubble was determined under the assumption that the sum of volumes of daughter bubbles is equal to the volume of the bubble that has been disintegrated.

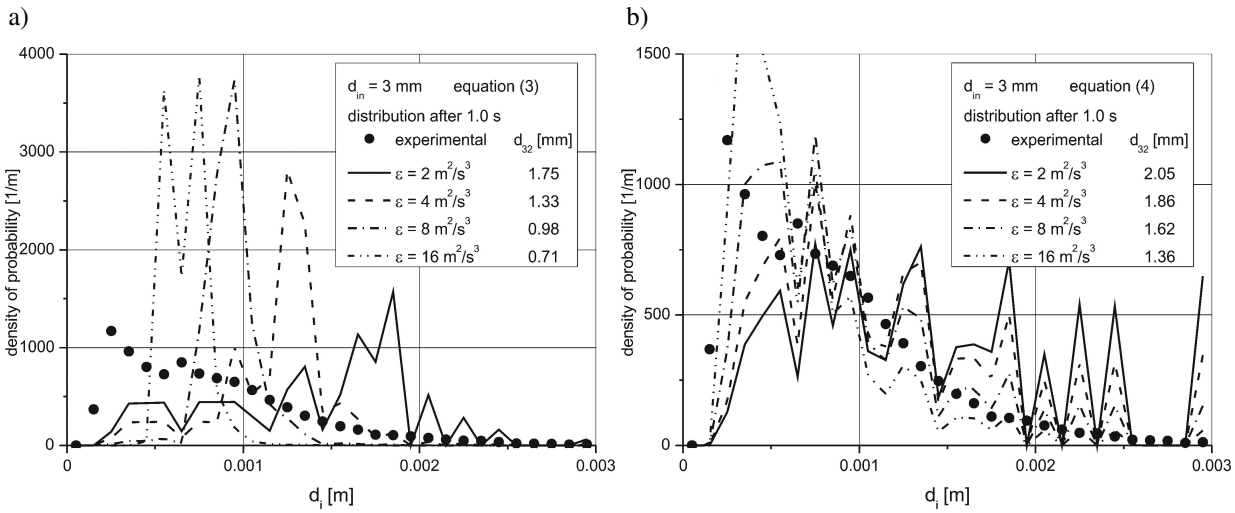

Fig. 7. Probability density distributions of bubble sizes for binary break-up: a) from Eq. (3) for d_{in} = 3 mm, b) from Eq. (4) for d_{in} = 3 mm

Better agreement between experimental and model data was obtained for Eq. (4). For the range from ε = 8 m^2/s^3 to ε = 16 m^2/s^3 good agreement between Sauter diameters determined experimentally and by modelling was also obtained. However, this agreement was obtained for break-up time of 1 s at ε = 16 m^2/s^3. This time is much longer than that determined on the basis of film analysis of the process. This leads to a conclusion confirming the observations and literature information that bubbles must be disintegrated into a larger number of daughter bubbles.

3.4. Bubble size distributions for break-up into 5 daughter bubbles

Because during bubble break-up into two daughter bubbles the modelled process takes too long compared to the reality, calculations based on Eq. (1) were made for the bubble break-up into 5 daughter bubbles. Simulation results for the imposed duration of break-up τ = 0.03 s and probability of obtaining daughter bubbles determined by Eqs. (3) and (6) are shown in Fig. 8. Good agreement of experimental and model data distribution was not obtained. This applies in particular to the position of peaks in the graph, which are shifting towards smaller diameters with increasing energy dissipation rates. However, for small values of $\varepsilon \approx 4$ m^2/s^3 there is agreement of Sauter diameters.

Better results were obtained for Eqs. (4) and (6) which is shown in Fig. 9. Agreement of the distribution of model and experimental results is quite good for the range from ε = 8 m^2/s^3 to ε = 16 m^2/s^3. There are local maxima for the model results, which, however, make the calculated Sauter diameters be higher than the experimental ones.

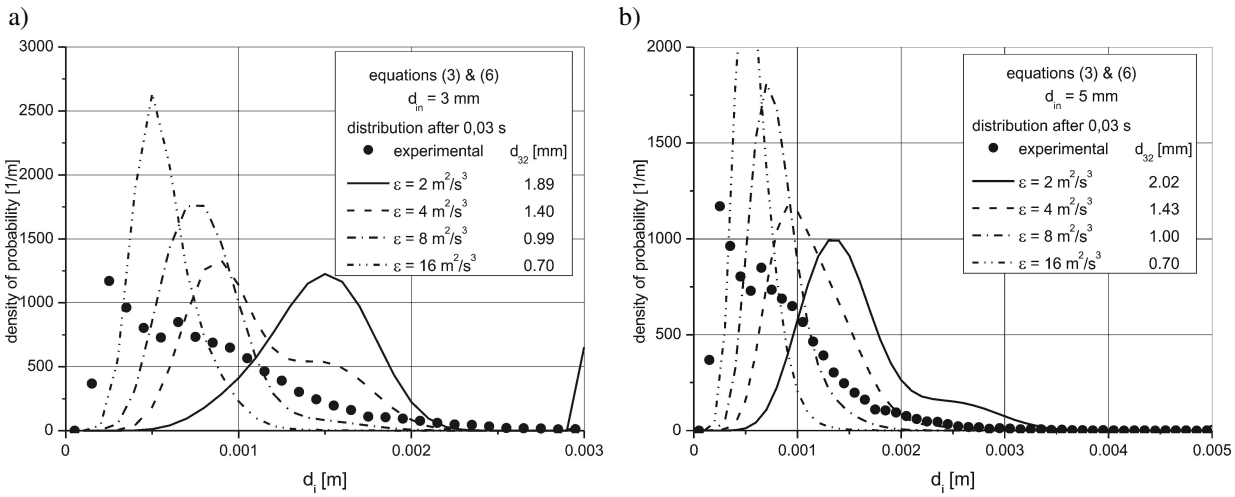

Fig. 8. Probability density distributions of bubble sizes from Eqs. (3) and (6) for break-up into 5 daughter bubbles: a) for the initial diameter of bubbles d_{in} = 3 mm, b) for the initial diameter of bubbles d_{in} = 5 mm

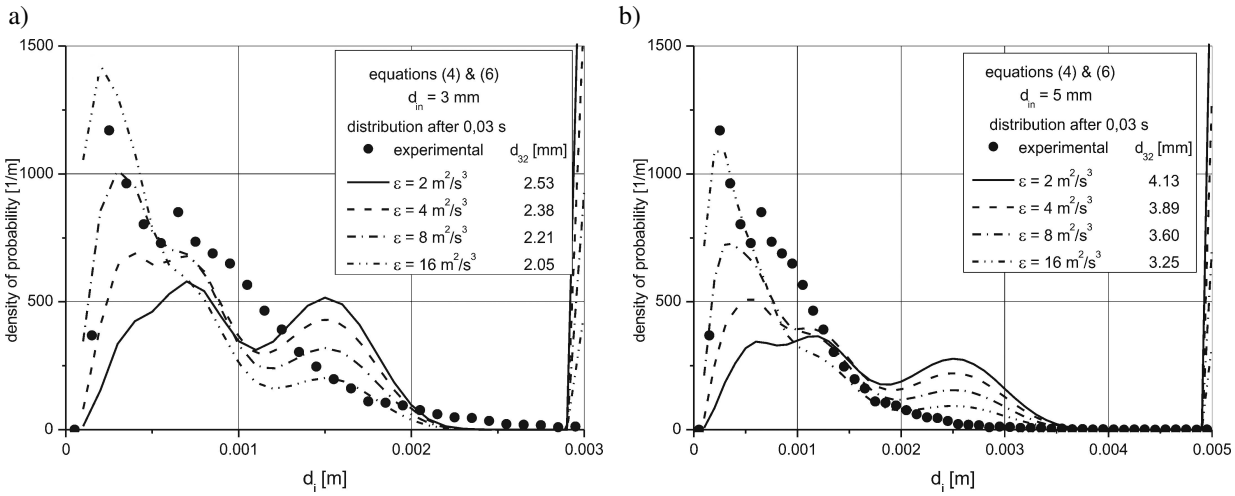

Fig. 9. Probability density distributions of bubble sizes from Eqs. (4) and (6) for break-up into 5 daughter bubbles: a) for the initial diameter of bubbles d_{in} = 3 mm, b) for the initial diameter of bubbles d_{in} = 5 mm

3.5. Bubble size distributions for break-up into a random number of bubbles

Calculations were carried out for the case when a primary bubble was disintegrated into a random number of daughter bubbles preserving the condition of equal volume of the daughter bubbles with the volume of the primary bubble. The number of daughter bubbles was from 2 to 5. In the case of random determination of the number of daughter bubbles, a detailed form of the bubble size distribution function $\beta(d_i, d_j)$ is not required.

Calculations were made for Equations (2), (3) and (4). Calculation results for Equation (2) are shown in Fig. 10. Due to random changes in the shape of curves, 10 curves were averaged.

For Eq. (2) good agreement of bubble size distributions was obtained for ε = 128 m^2/s^3 (for d_{in} = 5 mm compliance was quite good also for ε = 64 m^2/s^3) at the break-up time τ = 0.035 s, which is slightly longer than that previously determined. However, it is very unlikely for such a big instantaneous energy dissipation rate to occur frequently in the discussed area (Fig. 10 shows values averaged over time). In addition, for bubbles with the size close to d_{in}, high probability density results from the calculations, i.e. inlet bubbles are not disintegrated with a sufficient frequency. This is not consistent with observations.

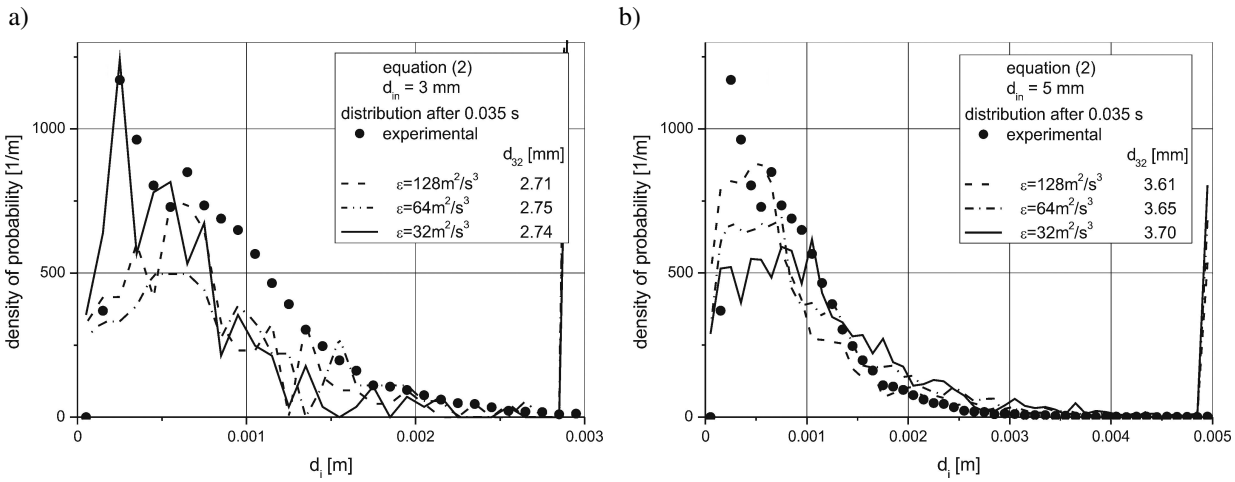

Fig. 10. Probability density distributions of bubble sizes from Eq. (2) for break-up into a random number of daughter bubbles: a) for the initial diameter of bubbles d_{in} = 3 mm, b) for the initial diameter of bubbles d_{in} = 5 mm

Figure 11 shows a comparison of experimental and model bubble size distributions calculated from Eq. (3). In this case, the best agreement occurs for ε = 64 m^2/s^3, so for the value that is not very likely near the blades of the impeller being tested.

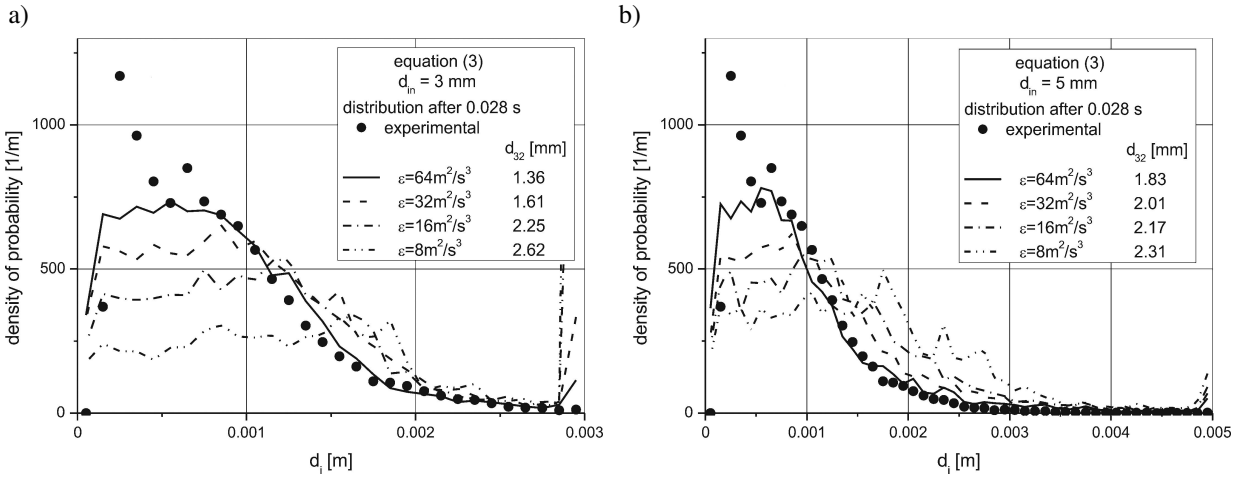

Fig. 11. Probability density distributions of bubble sizes from Eq. (3) for break-up into a random number of daughter bubbles: a) for the initial diameter of bubbles d_{in} = 3 mm, b) for the initial diameter of bubbles d_{in} = 5 mm

When dividing a bubble into a random number of daughter bubbles, getting a good match of Eqs. (2) and (3) to experimental data requires the use of very large values of energy dissipation rate (ε = 128 m^2/s^3). The probability of such values occurring near the self-aspirating disk impeller is very low. Therefore, in this case Eqs. (2) and (3) are useless.

For model calculations, high probability density values are characteristic for diameters close to the size of inlet bubbles. This means that many bubbles flowing out of the outlet orifices should not be disintegrated into smaller bubbles. In fact, the number of such large bubbles is very small, i.e. model conditions do not correspond to real conditions. Also in the case of small bubbles (d_i < 0.5 mm) the model disintegration rate is smaller than the real one. A slight improvement in this range of diameters can be obtained by increasing the number of daughter bubbles, as shown in Fig. 12.

Equation (4) shows higher rates of disintegration for d_i < 0.5 mm, but its use in the Monte Carlo method encountered difficulties. For d_{in} = 5 mm and ε = 16 m^2/s^3 the calculated bubble break-up rate is 5.954 s^{-1}.

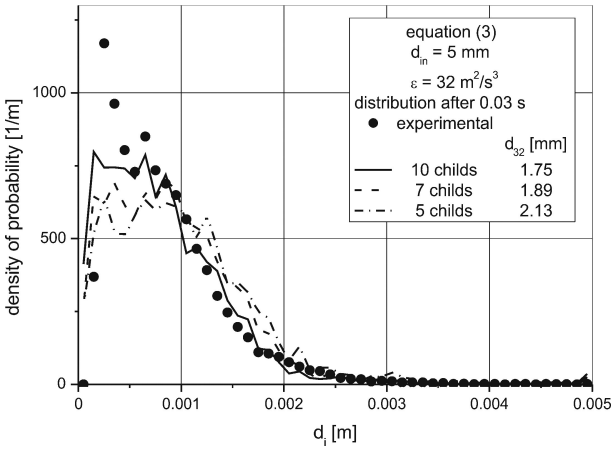

Fig. 12. Dependence of probability density distribution obtained from Eq. (3) by the MC method on the number of daughter bubbles

To perform at least several iterations for the break-up time $\tau = 0.03$ s the time interval must be about $\Delta\tau = 0.005$ s. Then the number of inlet bubbles to be disintegrated is 0.03, while in the Monte Carlo method the number must be an integer. In Eq. (1) bubble concentration in a unit of liquid volume is used, and therefore fractional values are acceptable and time interval can be even shorter. For this reason, it is not possible to perform calculations by the Monte Carlo method for the bubble disintegration rate described by Eq. (4).

4. CONCLUSIONS

Analysis of films obtained at a rate of 250 frames/s and with the image field covering the impeller vicinity showed (despite low resolution) that in the initial phase of gas dispersion by the self-aspirating impeller bubbles flowing out from outlet orifices were disintegrated by eddies formed behind the impeller blades. The process of disintegration lasts no longer than the time in which the blade makes 1/6 rotation. This time is a limitation for modelling bubble disintegration by eddies formed behind the blade.

Energy dissipation rates calculated from Eqs. (7) and (8) have very similar distributions but they differ in maximum values. Unfortunately, it cannot be concluded which of the methods/models gives better results. It can be assumed that the highest time-averaged values of ε in the analysed area should not exceed $\varepsilon = 25$ m^2/s^3. However, instantaneous values may exceed the number.

It follows from experimental studies and model calculations that bubble break-up by eddies formed behind the blades is not binary.

Calculations made for a simplified model of bubble population balance (Eq. (1)) assuming no coalescence) showed good agreement between the Laakkonen model (Eq. (4)) and experimental data. Unfortunately, the model could not be used in simulating the process with the Monte Carlo method.

When calculating bubble size distribution based on the Monte Carlo method, the best results were obtained on the basis of the Lehr model (Eq. (3)). However, to obtain better agreement of experimental and model data, the function of bubble break-up rate should give higher values for bubbles with diameters smaller than 0.5 mm.

The study was carried out within project no. Dz.St. 501/10-34-1-7118.

SYMBOLS

C	constant/coefficient
C_s	Smagorinsky constant
D	impeller diameter, m
d_i	middle of class i, m
Δd	width of the class, m
$g(d_i)$	break-up frequency of bubble of size d_i, s^{-1}
n_c	number of classes
u'	velocity pulsations, $m \cdot s^{-1}$
$\bar{u'}$	mean-square velocity pulsation, $m \cdot s^{-1}$
Y_i	number of bubbles in class i
$Y_{i,in}$	number of inlet bubbles in class i
$Y_{i,out}$	number of outflowing bubbles in class i
ε	energy dissipation rate, $m^2 \cdot s^{-3}$
η_C, η_D	dynamic viscosity coefficient of continuous and disperse phases, respectively, Pa·s
$\nu(d)$	number of bubbles formed during the division of bubble of size d
τ	time, s

Dimensionless numbers

$Re = \dfrac{N \cdot D^2 \cdot \rho}{\eta_C}$ Reynolds number for mixing process

$Fr' = \dfrac{N^2 \cdot D^2}{g \cdot (H - h)}$ modified Froude number for mixing process ($H-h$ – liquid height above impeller)

REFERENCES

Alopaeus V., Koskinen J., Keskinen K.I., 1999. Simulation of the population balances for liquid-liquid systems in a nonideal stirred tank. Part 1 Description and qualitative validation of the model. *Chem. Eng. Sci.*, 54, 5887–5899. DOI: 10.1016/S0009-2509(99)00170-0.

Attarakih M.M., Drumm C., Batr H.-J., 2009. Solution of the population balance equation using the sectional quadrature method of moments (SQMOM). *Chem. Eng. Sci.*, 64, 742–752. DOI: 10.1016/j.ces.2008.05.006.

van der Hengel E.I.V., Deen N.G., Kuipers J.A.M., 2005. Application of coalescence and breakup models in a discrete bubble model for bubble columns. *Ind. Eng. Chem. Res.*, 44, 5233–5245. DOI: 10.1021/ie0492449.

Kálal Z., Jahoda M., Fořt I., 2014. Modeling of the bubble size distribution in an aerated stirred tank: Theoretical and numerical comparison of different breakup models. *Chem. Process Eng.*, 35, 331–348. DOI: 10.2478/cpe-2014-0025.

Kania A., Kuncewicz C., 2002. Energy dissipation rate and the size of eddies in the tank with self-aspirating impeller. *15th International Congress of Chemical & Process Engineering* CHISA 2002, Praha.

Laakkonen M., Moilanen P., Alopaeus V., Aittamaa J., 2006. Modeling local gas-liquid mass transfer in agitated vessels. *12th European Conference on Mixing*, Bologna. 193–200.

Laakkonen M., Moilanen P., Alopaeus V., Aittamaa J., 2007. Modeling local bubble size distribution in agitated vessels. *Chem. Eng. Sci.*, 62, 721–740. DOI: 10.1016/j.ces.2006.10.006

Lehr F., Milles M., Mewes D., 2002. Bubble-size distributions and flow fields in bubble columns. *AIChE J.*, 48, 2426–2443. DOI: 10.1002/aic.690481103.

Luo H., Svendsen H.F., 1996. Theoretical model for drop and bubble breakup in turbulent dispersions. *AIChE J.*, 42, 1225–1233. DOI: 10.1002/aic.690420505.

Martinez-Bazán C., Montañés J.L., Lasheras J.C., 1999. On the breakup of an air bubble injected into a fully developed turbulent flow. Part 1. Breakup frequency. *J. Fluid Mech.*, 401, 183–207. DOI: 10.1017/S0022112099006680.

Paglianti A., Fujasowa M., Montante G., 2006. Experimental study and a mechanistic model on the effect of ventilated cavities in gassed stirred vessels. *12th European Conference on Mixing*, Bologna. 650–657.

Pohorecki R., Moniuk W., Zdrójkowski A., Bielski P., 2001a. Hydrodynamics of a pilot plant bubble column under elevated temperature and pressure. *Chem. Eng. Sci.*, 56, 1167–1174. DOI: 10.1016/S0009-2509(00)00336-5.

Pohorecki R., Moniuk W., Bielski P., Zdrójkowski A., 2001b. Modelling of the coalescence/redispersion processes in bubble columns. *Chem. Eng. Sci.*, 56, 6157–6164. DOI: 10.1016/S0009-2509(01)00214-7.

Stelmach J., 2000. Investigations of a self-aspirating disk impeller work. *Ph.D. thesis*, Lodz University of Technology, Lodz, Poland (in Polish).

Stelmach J., 2006. Bubble size in the initial phase of self-aspiration. *Inż. Apar. Chem.*, 6s, 225–227.

Stelmach J., 2007. Distribution of gas bubble sizes at the beginning of self-aspirating. *Inż. Apar. Chem.*, 4–5, 117–119.

Stelmach J., Kuncewicz C., 2011. Liqud and gas bubble velocities at the level of a self-aspirating disk impeller. *Przem. Chem.*, 90/9, 1680–1685.

Stelmach J., Kuncewicz C., Musoski R., 2016. Analysis of the mechanism of gas bubble break-up in liquids during the self-aspirating impeller operation. *Chem. Process Eng.*, 37, 441–457. DOI: 10.1515/cpe-2016-0037.

Stelmach J., Musoski R., Kuncewicz C., Głogowski M., 2019. Turbulent Energy dissipation rate and turbulence scales in the blade region of a self-aspirating disk impeller. *J. Appl. Fluid Mech.*, 12, 3, 715–728. DOI: 10.29252/jafm.12.03.28836.

Received 03 December 2019
Received in revised form 02 March 2020
Accepted 03 March 2020